Supplement of

Assessing the importance of nitric acid and ammonia for particle growth in the polluted boundary layer

Ruby Marten[1], Mao Xiao[1], Mingyi Wang[2], Weimeng Kong[2], Xu-Cheng He[3,4], Dominik Stolzenburg[3,5], Joschka Pfeifer[6,7], Guillaume Marie[7], Dongyu S. Wang[1], Andrea Baccarini[1,8], Chuan Ping Lee[1], Antonio Amorim[9], Rima Baalbaki[3], David M. Bell[1], Barbara Bertozzi[10], Lucía Caudillo[7], Lubna Dada[1], Jonathan Duplissy[3,11], Henning Finkenzeller[12], Martin Heinritzi[7], Markus Lampimäki[3], Katrianne Lehtipalo[3,4], Hanna E. Manninen[6], Bernhard Mentler[13], Antti Onnela[6], Tuukka Petäjä[3], Maxim Philippov[14], Birte Rörup[3], Wiebke Scholz[13], Jiali Shen[3], Yee Jun Tham[3], António Tomé[15], Andrea C. Wagner[7,12,16], Stefan K. Weber[6,7], Marcel Zauner-Wieczorek[7], Joachim Curtius[7], Markku Kulmala[3], Rainer Volkamer[12], Douglas R. Worsnop[3,17], Josef Dommen[1], Richard C. Flagan[2], Jasper Kirkby[6,7], Neil McPherson Donahue[18], Houssni Lamkaddam[1,@], Urs Baltensperger[1], Imad El Haddad[1,@]

[1]Laboratory of Atmospheric Chemistry, Paul Scherrer Institute, 5232 Villigen, Switzerland.
[2]California Institute of Technology, Division of Chemistry and Chemical Engineering 210-41, Pasadena, CA 91125, USA.
[3]Institute for Atmospheric and Earth System Research (INAR)/ Helsinki Institute of Physics, Faculty of Science, University of Helsinki, 00014 Helsinki, Finland.
[4]Finnish Meteorological Institute, FI-00560 Helsinki, Finland
[5]Institute for Materials Chemistry, TU Wien, 1060 Vienna, Austria
[6]CERN, CH-1211 Geneva, Switzerland.
[7]Institute for Atmospheric and Environmental Sciences, Goethe University Frankfurt, 60438 Frankfurt am Main, Germany.
[8]Atmospheric Processes and their Impact, École Polytechnique Fédérale de Lausanne, 1015 Lausanne, CH.
[9]CENTRA and FCUL, University of Lisbon, 1749-016 Lisbon, Portugal.
[10]Institute of Meteorology and Climate Research, Karlsruhe Institute of Technology, 76021 Karlsruhe, Germany.
[11]Helsinki Institute of Physics (HIP)/Physics, Faculty of Science, University of Helsinki, 00014 Helsinki, Finland
[12]Department of Chemistry & CIRES, University of Colorado Boulder, 215 UCB, Boulder, 80309, CO, USA.
[13]Institute of Ion Physics and Applied Physics, University of Innsbruck, 6020 Innsbruck, Austria
[14]Lebedev Physical Institute of the Russian Academy of Sciences, 119991, Moscow, Leninsky prospekt, 53, Russian Federation.
[15]IDL-Universidade da Beira Interior, 6201-001 Covilhã, Portugal.
[16]Aerosol Physics Laboratory, Physics Unit, Tampere University, FI-33014 Tampere, Finland
[17]Aerodyne Research, 01821 Billerica, MA, USA
[18]Center for Atmospheric Particle Studies, Carnegie Mellon University, 1521 Pittsburgh, PA, USA.

[@]Corresponding authors e-mails: houssni.lamkaddam@psi.ch, imad.el-haddad@psi.ch

Summary

This supplementary information (SI) section presents supplementary figures exploring growth by N_2O_5, sensitivity tests of the kinetic model, particle composition outputs from the model, and model results with the resolution of a long scanning mobility particle sizer (lSMPS).

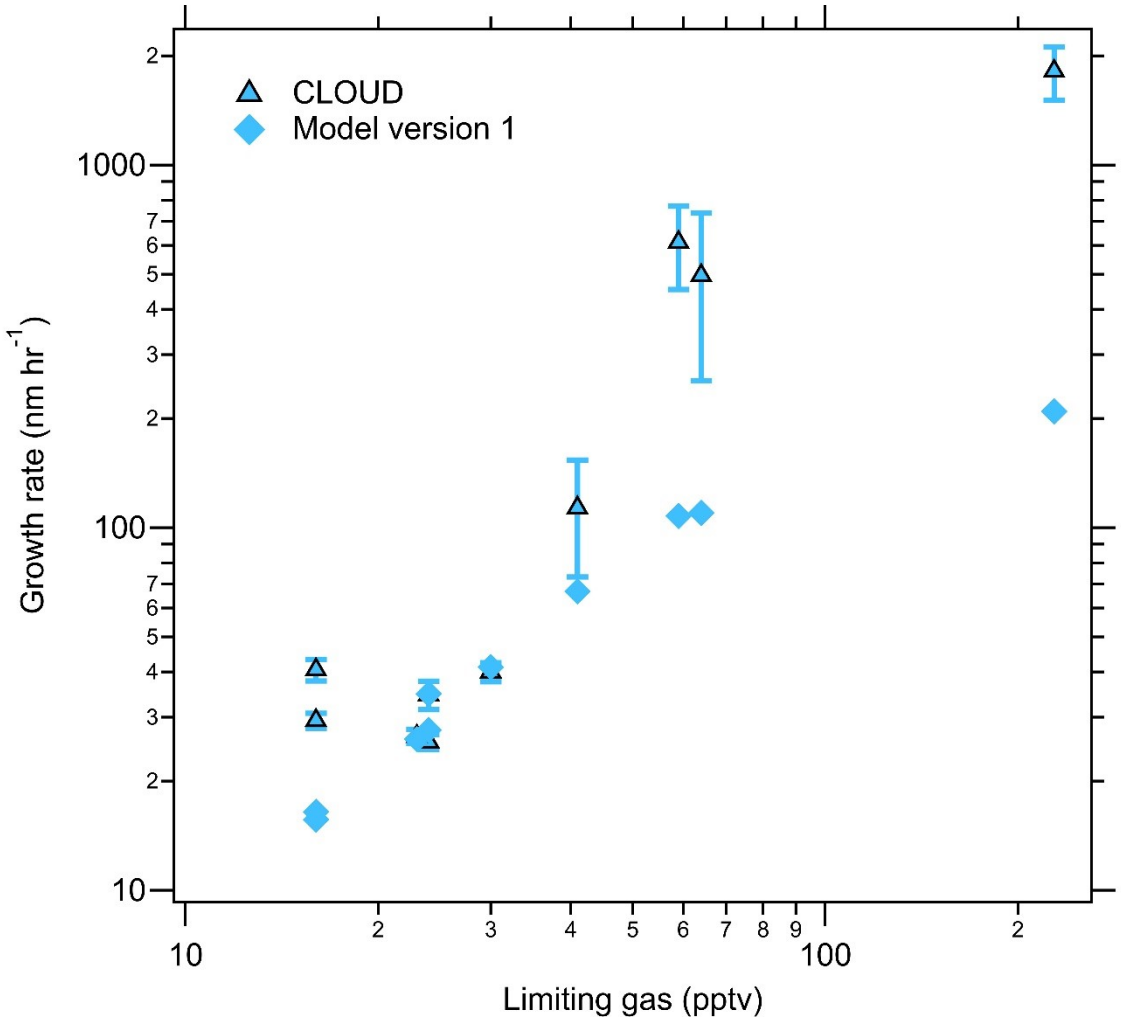

Figure S1 : Growth rates using input of HNO_3 as the limiting gas. *All of the -10°C runs were limited by HNO_3, these modelled growth rates are calculated using only the measured HNO_3 concentration, whereas for the model results presented in Fig. 1 the concentration of N_2O_5 was added to the HNO_3 concentration for the model constraints. Including the N_2O_5 concentrations in the model brought the model and measured growth rates closer together, and also shifted the points right on the x-axis since the gas concentration was increased.*

Table S1: Data from figure S1. *N_2O_5 was modelled assuming that it has the same wall and condensation sink losses as HNO_3 and H_2SO_4.*

Run	Limiting gas / pptv	GR / nm hr^{-1}	N_2O_5 / pptv	N_2O_5 / pptv assuming no wall loss
1	228	1814.3	150	1300
2	64	495.6	24	196
3	41	113.41	17	150
4	59	611.97	9	370
5	24	25.65	2e-2	0.1
6	24	34.6	2e-2	0.1

7	23	26.6	1e-2	2e-2
8	30	40.01	2e-2	6e-2
9	16	29.39	3e-3	2e-2
10	16	40.54	1e-2	0.1

$$Flux_A = v_{dep} \div h_{BL} \quad \text{(S1)}$$
$$p_A = [A_i] \times Flux_A \quad \text{(S2)}$$

We calculated suitable production values of HNO_3, NH_3, and H_2SO_4 based on the required steady-state concentration in the absence of condensation. The vertical dry deposition fluxes of gas A, $Flux_A$, were calculated using equation S1 with literature deposition velocities, v_{dep}, for HNO_3, NH_3, and H_2SO_4, shown in Table S2. The height of the boundary layer, h_{BL}, used was 1km. The production values of HNO_3 and NH_3 were calculated using equation S2 from the deposition flux, and initial concentration of A, $[A_i]$, considering the deposition flux as the highest loss rate for both gases. The production rate of H_2SO_4 was calculated considering new particle formation as the highest loss rate of gaseous H_2SO_4. The initial concentrations and production rates for the experiments in sections "Effect of inhomogeneity of NH_3 concentrations in cities" and "Effect of temperature change during vertical transport" are shown in Table S2.

Table S2: Calculation of diffusion losses

Gas	Simulation	T/°C	Deposition Velocity v_{dep} / cm s^{-1}	Boundary layer height / cm	Initial concentration	Production rate / molecules cm^{-3} s^{-1}
HNO_3	Temperature change	15	4[1]	100,000	1 ppbv	1.1×10^6
NH_3	Temperature change	15	2[2]	100,000	3 ppbv	1.6×10^6
H_2SO_4	Temperature change	15	1.5[1]	100,000	1×10^7 molecules cm^{-3}	1.6×10^5
HNO_3	NH_3 inhomogeneities	5	4[1]	100,000	0.2 ppbv	3.3×10^5
NH_3	NH_3 inhomogeneities	5	2[2]	100,000	1 ppbv	6.5×10^5
H_2SO_4	NH_3 inhomogeneities	5	1.5[1]	100,000	1×10^7 molecules cm^{-3}	2.2×10^5

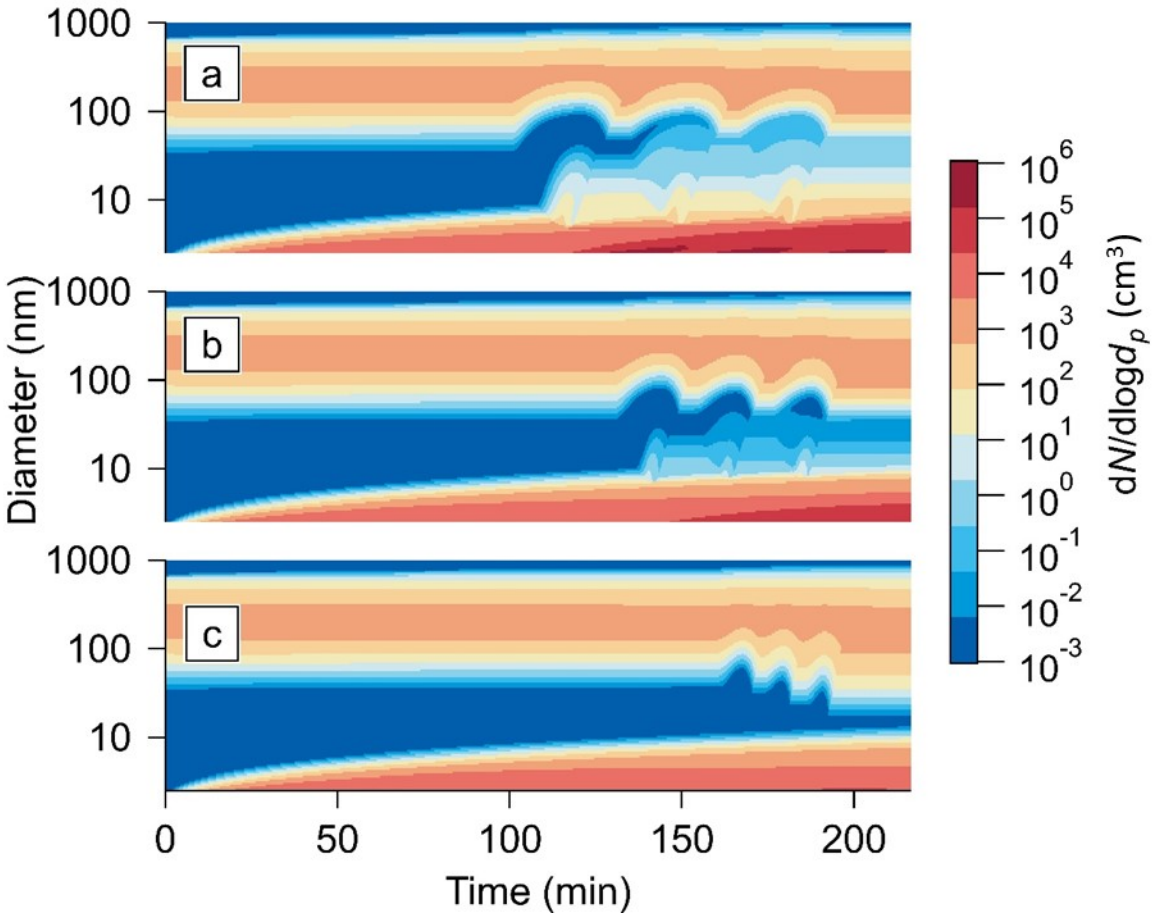

Figure S2: Temperature change sensitivity tests. *All model Initial conditions are 3 ppbv NH_3, 1 ppbv HNO_3 and 1 × 10^7 molecules cm^{-3} H_2SO_4.* ***a)*** *Repeat of model presented in Fig. 2c) with a change in temperature of 15°C from 15°C to 0°C. Displayed here for comparison.* ***b)*** *Repeat of a) but with a temperature change of 10°C from 15°C to 5°C.* ***c)*** *Repeat of a) with a temperature change of 5°C from 15°C to 10°C. It is clear that a larger temperature change results in a bigger change to the nucleation mode.*

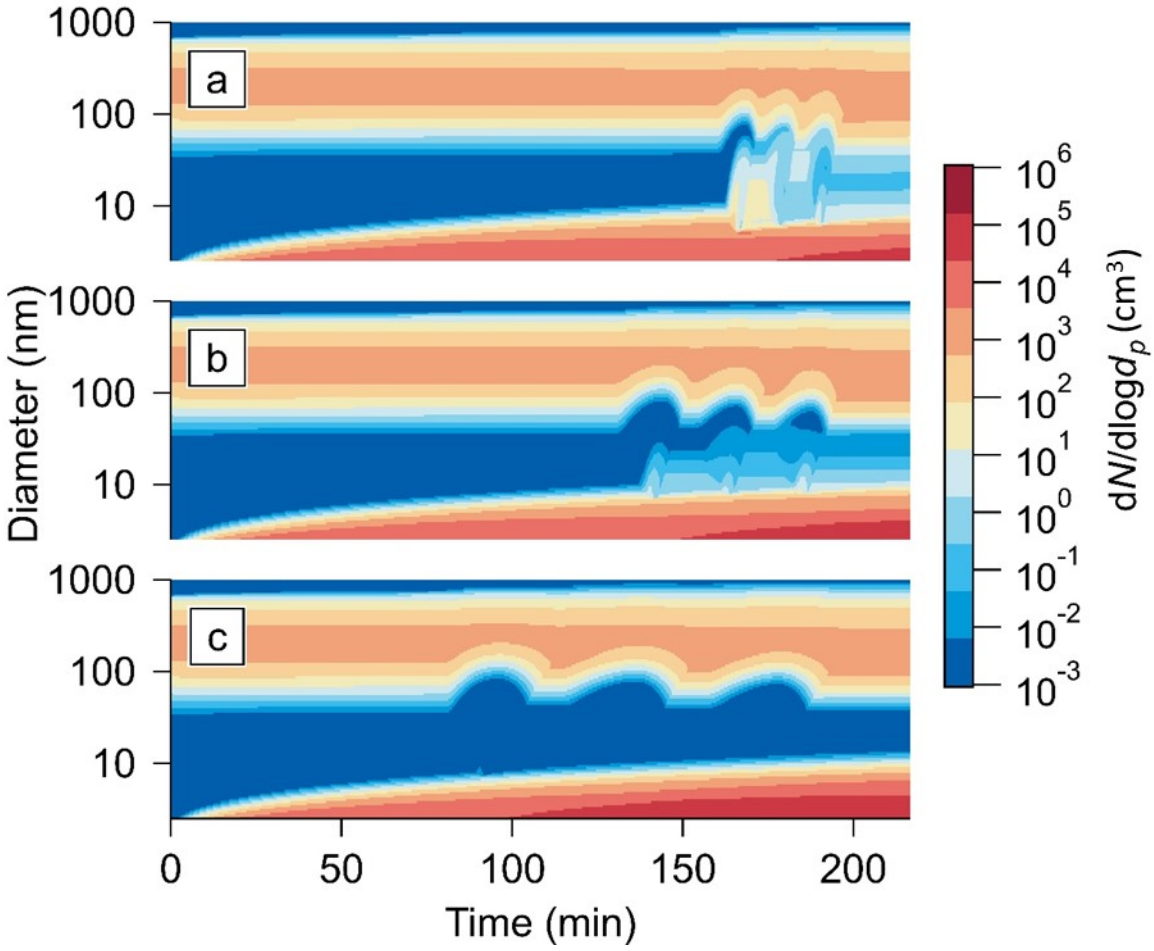

Figure S3: Rate of temperature change sensitivity tests. *All model initial conditions are 3 ppbv NH_3, 1 ppbv HNO_3 and 1 × 10^7 molecules cm^{-3} H_2SO_4.* ***a)*** *Model results with a temperature change of 10°C from 15°C to 5°C over 5 minutes.* ***b)*** *Repeat of Figure S2b) Model results with a temperature change of 10°C from 15°C to 5°C over 10 minutes. Displayed here for comparison.* ***c)*** *Model results with a temperature change of 10°C from 15°C to 5°C over 20 minutes. This shows that the temperature change must be fast to affect the growing particles.*

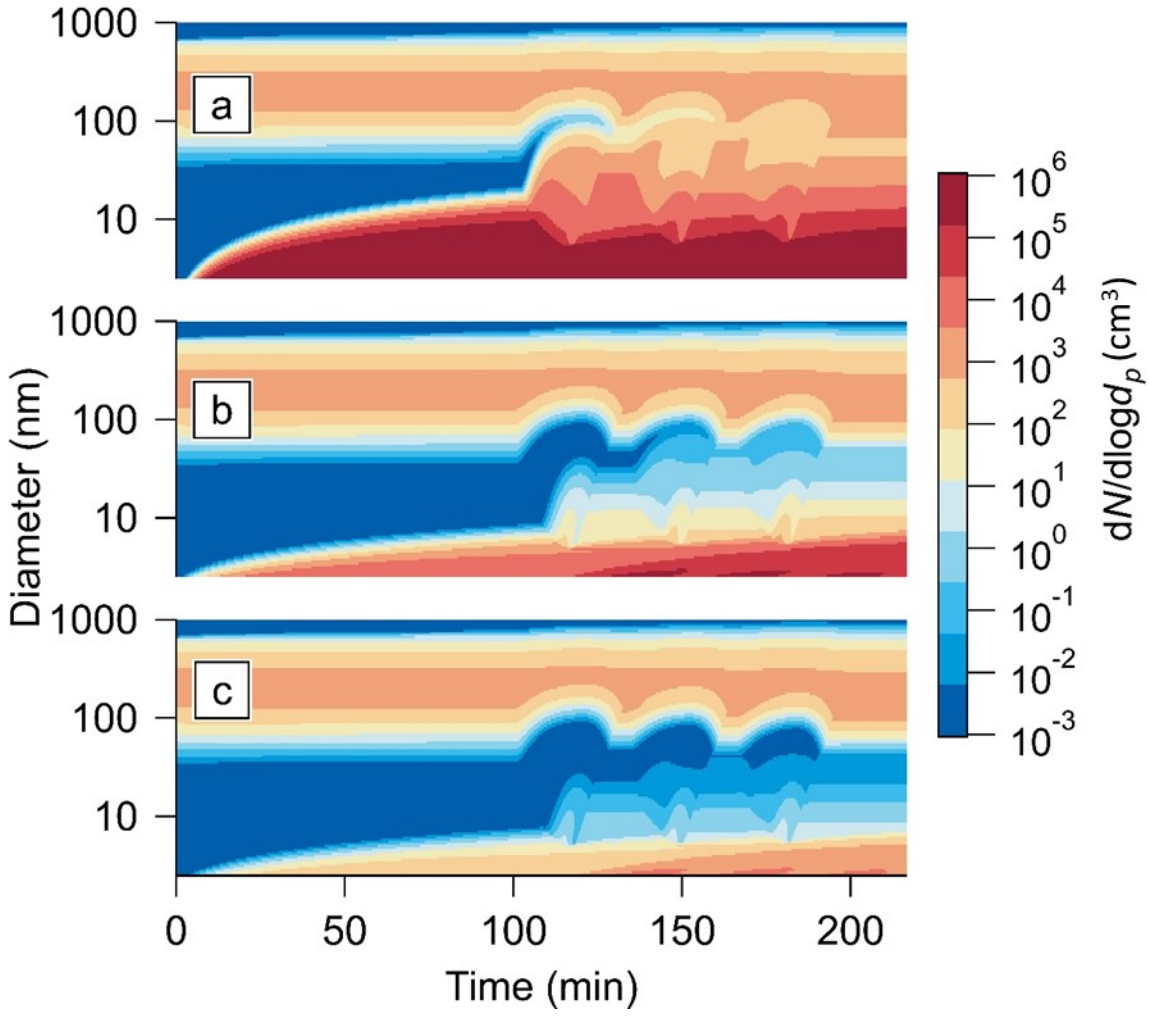

Figure S4: Nucleation rate sensitivity tests. a) *Model results with a temperature change of 15°C from 15°C to 0°C with kinetic nucleation rates.* ***b)*** *Repeat of model presented in Fig. 2c) with a change in temperature of 15°C from 15°C to 0°C. Displayed here for comparison.* ***c)*** *Repeat of b) but with fifty times lower nucleation rates. Since the nucleation rate affects the pre-existing particle distribution at the time of activation, a lower nucleation rate can result in activation of fewer particles.*

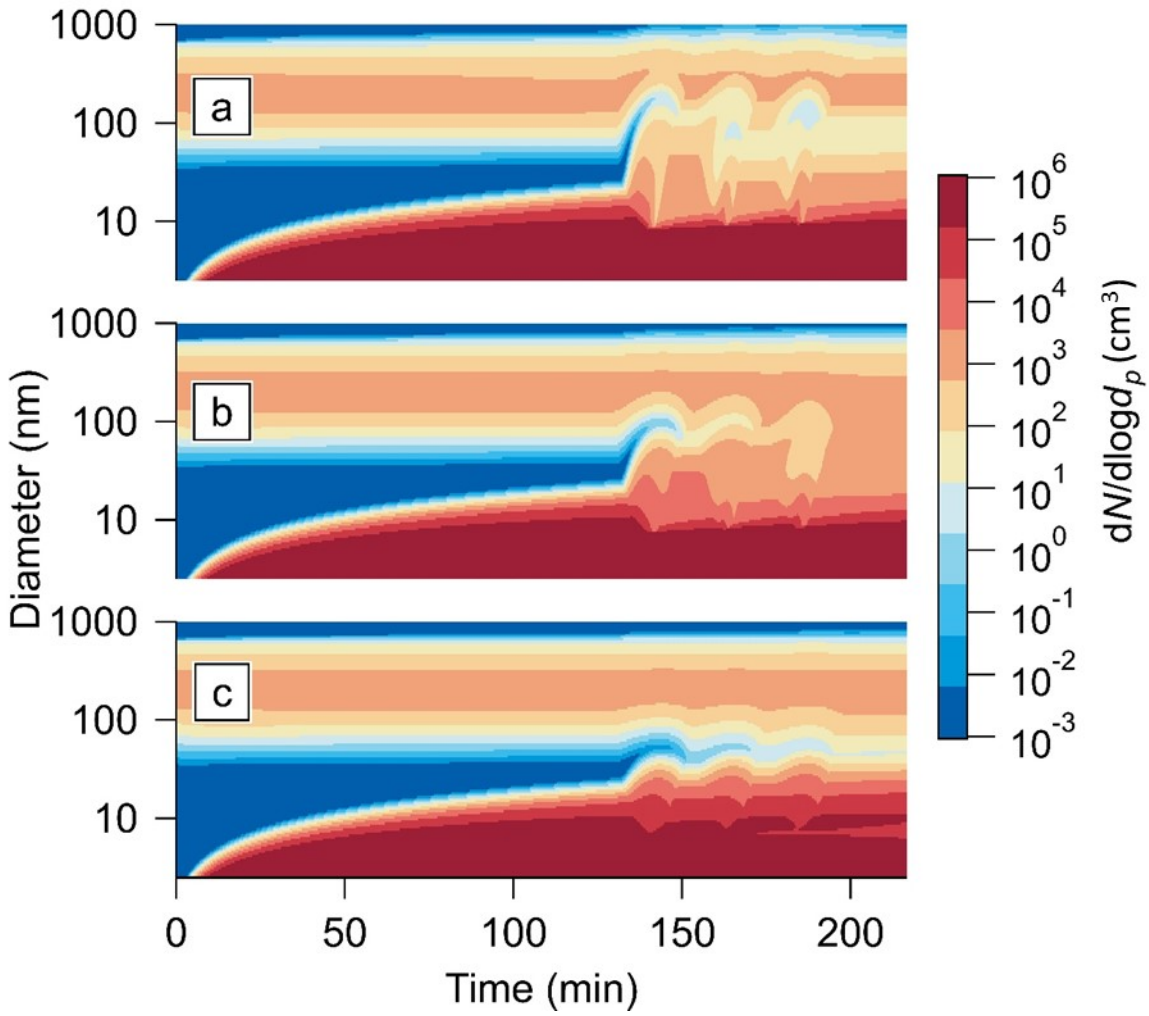

Figure S5: Initial temperature sensitivity tests. a) *Model results with a temperature change of 10°C from 20°C to 10°C with kinetic nucleation rates.* ***b)*** *Model results with a temperature change of 10°C from 15°C to 5°C with kinetic nucleation rates.* ***c)*** *Model results with a temperature change of 10°C from 10°C to 0°C with kinetic nucleation rates.*

Figure S6 shows the relationship of the dissociation constant, K_p, with temperature. It can be seen that in steady-state conditions, where the product of concentrations of gas phase NH_3 and HNO_3 are equal to the saturation temperature, a change in 10°C from 20°C to 10°C results in more available gas to condense than for 10°C to 0°C. K_p can be calculated by integrating the van't Hoff equation [3]. Equation S.1 shows the equation for K_p in units of ppb^2 (assuming 1 atm of total pressure) [4].

$$lnK_p = 118.87 - \frac{24{,}084}{T} - 6.025\ lnT \qquad \text{(S.1)}$$

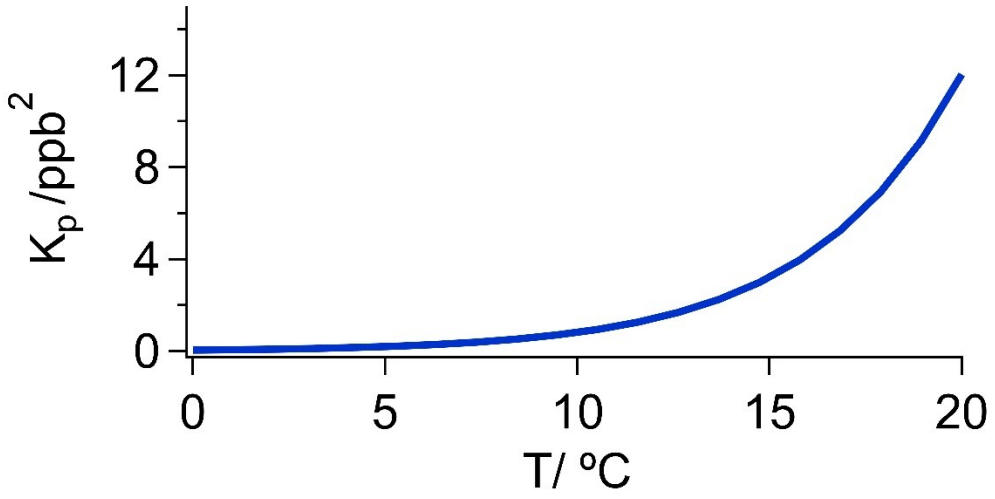

Figure S6: Dissociation constant of NH_4NO_3 (K_p/ppb^2) vs temperature (T/°C).

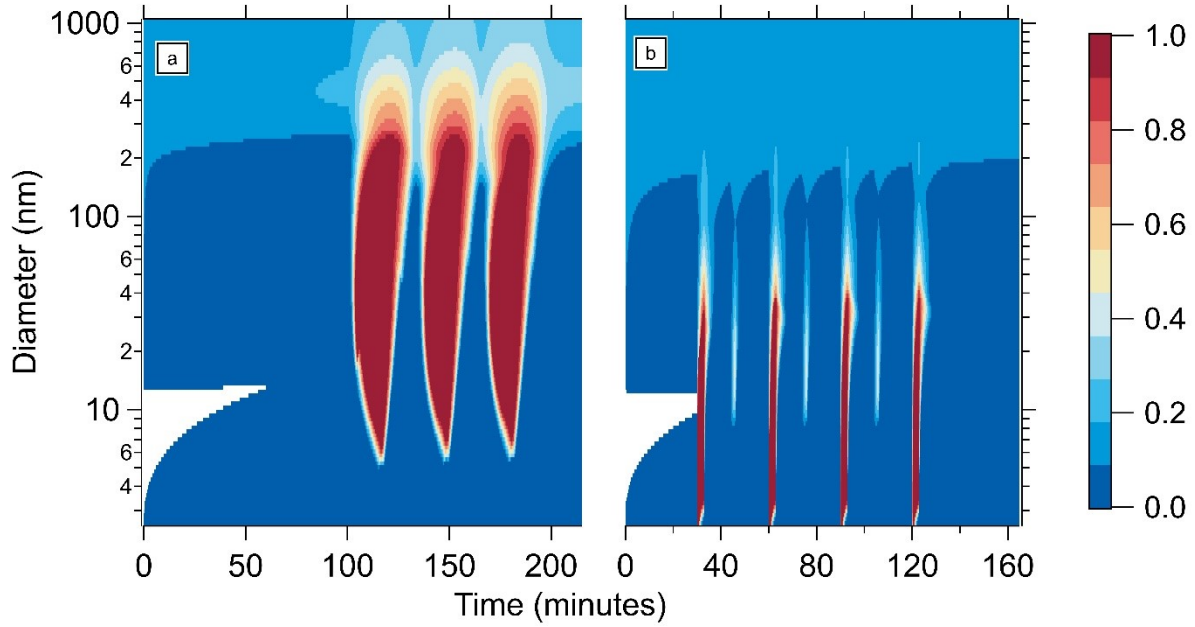

Figure S7: Number fraction of NH_4NO_3 from Fig. 2 and Fig. 3 as a function of time. *Number fraction is defined as the number concentration ratio (molecules cm^{-3} / total molecules cm^{-3}). The simulated condensation sink starts with 10% NH_4NO_3 and the inputs of NH_3 and HNO_3 are saturated at 200 nm (i.e. 200 nm is the activation diameter).* ***a)*** *Model results from Fig. 2c) (temperature change due to vertical transport).* ***b)*** *Model results from Fig. 3c) (inhomogeneities due to spikes of NH_3). The white colour represents absence of particles.*

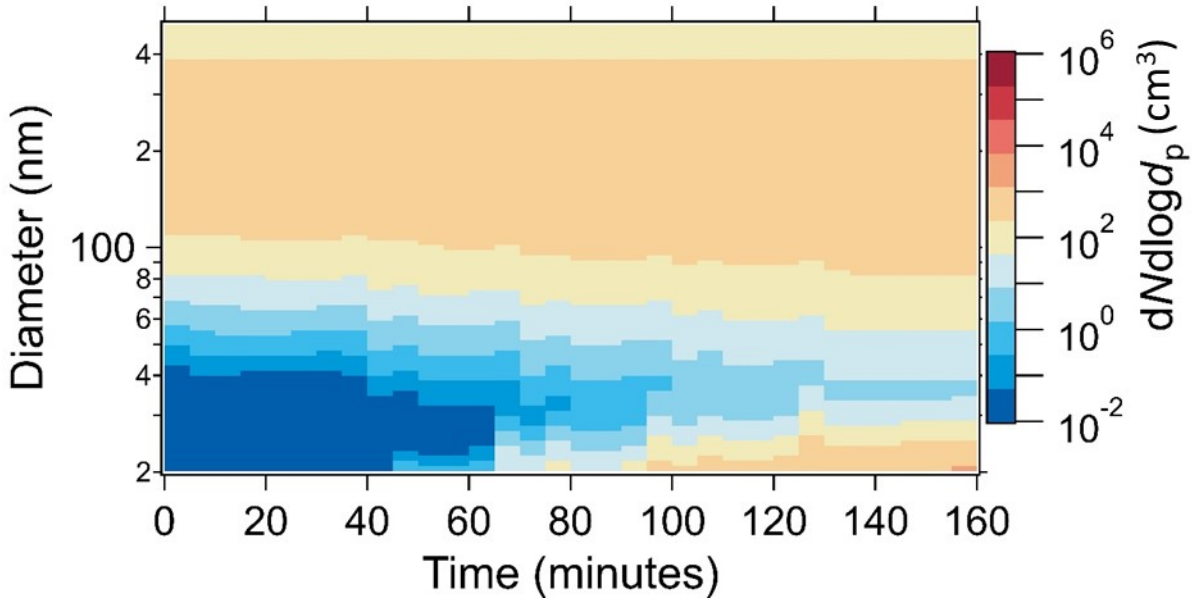

Figure S8: Low-resolution replication of Fig. 3b). *The size distribution from the model output presented in Fig. 3b) was interpolated to the size bins of the long SMPS (89 logarithmically spaced size bins 20-480 nm) and 5-minute time resolution. This illustrates that inhomogeneities may not be as noticeable in ambient measurements.*

References

1 J. Seinfeld H. and S. Pandis N., *Atmospheric Chemistry and Physics*, John Wiley & Sons, 2006, vol. 2nd edn.

2 R. San Jose, F. J. Moreno and M. A. San Feliu, eds. P. Fabian, V. Klein, M. Tacke, K. Weber and C. Werner, Munich, Germany, 1995, pp. 274–285.

3 K. G. Denbigh, *The Principles of Chemical Equilibrium: With Applications in Chemistry and Chemical Eengineering*, Cambridge University Press, 1981.

4 M. Mozurkewich, *Atmospheric Environment. Part A. General Topics*, 1993, **27**, 261–270.